Analysis of an MRI Compatible Force Sensor for Sensitivity and Precision

Melih Turkseven and Jun Ueda

***Abstract*—MRI compatible force sensors are important components in medical robotics as they enable force feedback in a challenging environment for surgical and assistive robots. This paper analyzes a novel MRI compatible force sensor comprised of a displacement amplifying compliant mechanism (DACM) made of polymers. Hysteresis is an inevitable problem for sensors made of polymers which reduces the precision in measurements. Displacement amplification affects both the sensitivity and hysteresis error of a sensor, yet does not ensure an improvement in either of them. Optimization methods based solely on amplification ratio or sensitivity may be ineffective on reducing the hysteresis issue and result in a design with insufficient signal-to-noise ratio (SNR). Unlike previous works that are focused on optimizing topologies with regard to a specific objective function; this work presents an analysis that accounts for both sensitivity and hysteresis. An iterative method capable of performing nonlinear analysis is established in order to monitor sensitivity and hysteresis error of the proposed sensor topology and find out how those are affected by the amplification. Optimal configurations for sensitivity and precision are deduced and the predictions made by the analysis are confirmed by experiments. This study indicated that sensitivity of a compliant mechanism could be traded for a lower hysteresis error i.e. higher precision. DACMs could be targeted to achieve a low hysteresis error rather than improving the sensitivity in a sensor. Compared to a non-amplifying, basis structure our proposed design achieved a 3-4 times higher SNR, mostly due to its higher precision.**

***Index Terms*—MRI compatible, amplification mechanism, hysteresis, sensitivity**

I. Introduction

A. Background

MAGNETIC Resonance Imaging (MRI) is a widely used technique in diagnostics because of its ability to monitor human soft tissue 3-D in real time. MRI-compatible devices, including medical instruments [1] and robots [2], [3], are expected to extend the capability of MRI to provide advanced intervention and tele-surgery. MRI compatible force sensors, in particular, have an impact on MRI's versatility as they enable haptic force feedback to be used in experiments regarding the brain's motor function or provide surgeons with force feedback during tele-operated surgeries.

Due to the intense magnetic field in the MRI room conventional designs that involve metals or employ electricity reduce the quality of the MRI images. Several force sensors with limited MRI compatibility have been developed compromising the range of applications [4], [5], [6]. Optical force sensors with compliant, plastic structures have been proposed for ultimate MRI compatibility. In such sensors, an applied force results in a particular deformation on a compliant body and the deformation is sensed by an optical aperture. The compliant body of a sensor could be shaped so as to match the type of sensing task [7], [8], [9], [10], [11], [12]. To have desired deformation characteristics and meet various application-dependent requirements such as sensitivity and multi-directionality, the idea of displacement amplifying compliant mechanisms (DACM) has been applied to the optical force sensors [13]. Polymers are often the material of choice for the mechanism in such designs for higher MRI compatibility and flexibility. MRI compatibilities of various materials are compared and superiority of polymers have been demonstrated by MRI images in Schenck's work [14]. Flexibility is a measure of allowable elastic deformation on a material defined as the ratio of its yield strength to its elastic modulus by Howell [15]. Polymers have the highest flexibility compared to other materials such as metals and ceramics. However, the non-linear stress-strain relationship and a high possibility of inaccuracy due to hysteresis are major problems with polymers that should be considered in designing a mechanism.

Several methods for improving plastic DACMs have been introduced in the last two decades [16], [17], [18], [19], [20], [21]. A great deal of work is based on what is called "topology optimization" in which an approximate topology of an efficient mechanism is obtained from a ground structure. The performance of a topology is defined by a custom function and an extremum of the function is calculated in consideration with several constraints defined by the designer.

Despite the fact that topology optimization methods are widely applied for amplification mechanism design, more specific analysis methods are available to incorporate size and shape optimization once the topology of the structure is determined [22], [23], [24], [25], [26], [27]. An analytical method based on the calculation of deflections by discretizing the body has been explained in Howell's book [15]. The body of the structure is modeled as a chain of beams and the deflection in each beam is predicted by utilizing Castigliano's theorem.

Most of the works related to DACM analysis are aimed to optimize the mechanisms of actuation. However, the primary desired qualities change when it comes to compliant bodies for sensing tasks. Sensitivity and precision of a deformable body become more important than the amplification of the mechanism. Ananthasuresh and Krishnan developed a general method for estimating the sensitivity of a given topology and compared several existing designs [28]. They introduced a

Manuscript received May 29, 2012; revised August 8, 2012. This work was supported in part by the National Science Foundation Engineering Center for Compact and Efficient Fluid Power (CCEFP).

Melih Turkseven and Jun Ueda are with George W. Woodruff School of Mechanical Engineering, Georgia Institute of Technology, Atlanta, GA, 30332-0405 U.S.A. (e-mail: mturkseven3@gatech.edu & jun.ueda@me.gatech.edu).

variable which they called “unloaded output sensitivity” to define the sensing performance of a force sensor. Then they synthesized a new mechanism using that new variable as the target to be maximized in the size and shape optimization step.

Wang and Hu developed a force/weight sensor that employs a quartz-crystal resonator (QCR) for the transduction and a compliant body [29]. A measure of sensitivity is derived analytically in their work. They maximize an objective function which is the ratio of sensitivity to measurement range.

B. Problem Statement

The idea of displacement amplification via compliant mechanisms (DACM) has been tailored for sensors aiming to increase the sensitivity. However, a kinematic amplification comes with a mechanical loss, meaning an increase in the stiffness of the deforming body. Also displacement amplification may require a complicated topology which may further propagate its stiffness. Therefore DACMs, even the ones with optimized topologies, may not be advantageous in sensitivity compared to non-amplifying, simple, flexible bodies. Additionally since displacement amplification modifies the deformation pattern, the amount of strain energy required for a certain output displacement is affected. Strain energy absorbed by a flexible body is related to its hysteresis error; higher the absorbed strain energy, more severe the hysteresis loss [30], [31]. The performance of the displacement amplifying mechanism is important in both sensitivity and hysteresis aspects between which there is no straightforward relation.

There is an extant work on optimization of DACM sensors with regard to amplification or sensitivity, yet the combined effects of displacement amplification on both sensitivity and precision have not been evaluated. A popular method for designing a DACM for sensors is to apply topology optimization based on the amplification ratio of the mechanism and to adjust the dimensions of the members that are unrealistic due to manufacturing constraints [20], [17]. In some recent works, topologies optimized with regard to amplification ratio are subjected to another optimization routine with a more application specific objective [28], [29]. However, the effects of using DACM on the hysteresis error of sensors have not been addressed in the literature. Loss of precision caused by hysteresis, which is a common problem in plastic materials [32], [12], [33], results in a poorer Signal-to-Noise Ratio (SNR) for a sensor. Focusing on optimizing a selected objective function that is based on sensitivity or amplification ratio does not take the hysteresis aspect into account. Considering the potential adverse effects of using DACM such as lower sensitivity or higher hysteresis error, the advantages of a DACM over a simple, non-amplifying topology deserves an evaluation which is not the object of previous works based on optimization.

In this work, a polymer based force sensor with a DACM topology, shown in Fig. 1, is analyzed for both sensitivity and hysteresis. This topology has been proven to be robust in force sensing as it can decouple off-axis disturbances [33]. The performance of this proposed design is evaluated by varying the amplification factor of the topology and monitoring the changes in strain energy, which is related to hysteresis error, and output stiffness, which represents the inverse of sensitivity. Our analysis yielded the relation among amplification ratio, sensitivity and hysteresis to be utilized for an improved signal-to-noise ratio (SNR). To have a fair discussion on the benefits of the proposed design, it is compared to a primitive, low-amplification and low-stiffness, basic structure. The validity of the discussions is checked by experiments.

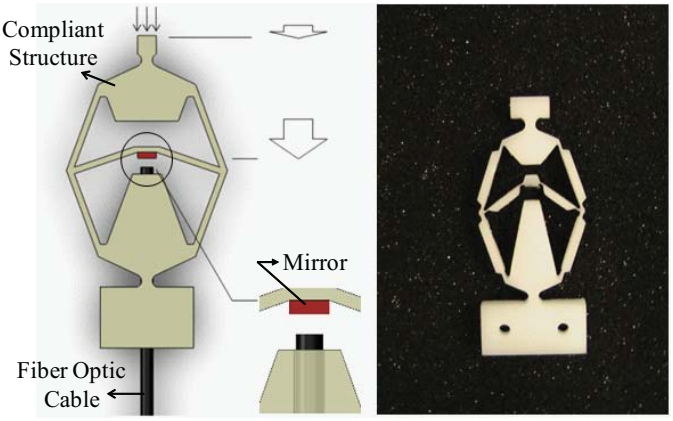

Fig. 1. MRI compatible optical force sensor. The Schematic (on the left) shows the working principle, a photo of delrin sample manufactured using a water-jet cutter (on the right).

The deformation of the compliant structure is computed via an algorithm capable of performing a nonlinear analysis. Instantaneous deformations can be estimated using Castigliano’s theorem which has been well implemented for compliant mechanisms by Howell [15]. In aforementioned works Howell’s method could be directly applied since the deformation is small enough to be assumed as linear. Unlike those works, in this application, the maximum output displacement is achieved by a non-linear deformation which requires a numeric algorithm that is capable of performing non-linear analysis. The established algorithm employs Howell’s method iteratively and updates the state of the deformed body after each iteration for a better accuracy.

II. Method

The analytical model established in this work is based on an iterative method capable of performing nonlinear analysis. The final deformed state of the compliant structure is estimated in iterations, applying the load incrementally (a common practice to mitigate the errors associated with geometric changes during the deformation). The load-deformation relationship is predicted using Castigliano’s displacement theorem. The performance of the sensor is evaluated by its amplification ratio, output stiffness and total strain energy.

The deflection at the output port of the mechanism is obtained using a method called “chain algorithm” which is explained in Howell’s book [15] in detail. In this method, the body is discretized into beam members. The discretized body of the proposed force sensor as well as the model of one arbitrary beam is shown in Fig. 2. Individual deformations of each beam member are calculated as if those members were cantilevered beams. At an arbitrary j^{th} iteration, location of

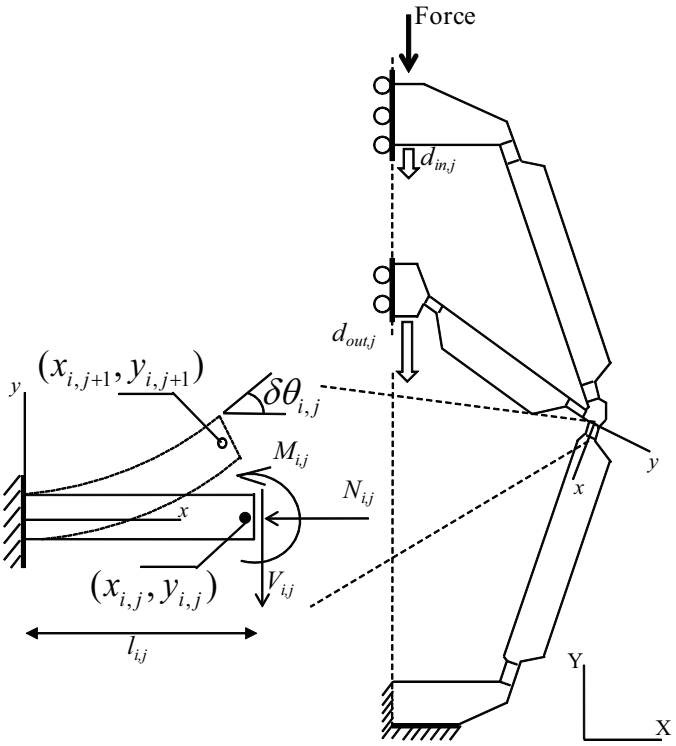

Fig. 2. Symmetric half of the proposed mechanism. Each member of the structure is modeled as a cantilevered beam (on the left).

the tip of the i^{th} beam member ($x_{i,j+1}$,$y_{i,j+1}$) is calculated using Castigliano's displacement theorem:

$$\delta x_{i,j} = \int_0^{l_{i,j}} \frac{M_{i,j}}{EA_i}\frac{\partial M_{i,j}}{\partial F_{x_{i,j}}}dx + \int_0^{l_{i,j}} \frac{N_{i,j}}{EA_i}\frac{\partial N_{i,j}}{\partial F_{x_{i,j}}}dx + \int_0^{l_{i,j}} \frac{kV_{i,j}}{GA_i}\frac{\partial V_{i,j}}{\partial F_{x_{i,j}}}dx \quad (1)$$

$$\delta y_{i,j} = \int_0^{l_{i,j}} \frac{M_{i,j}}{EA_i}\frac{\partial M_{i,j}}{\partial F_{y_{i,j}}}dx + \int_0^{l_{i,j}} \frac{N_{i,j}}{EA_i}\frac{\partial N_{i,j}}{\partial F_{y_{i,j}}}dx + \int_0^{l_{i,j}} \frac{kV_{i,j}}{GA_i}\frac{\partial V_{i,j}}{\partial F_{y_{i,j}}}dx \quad (2)$$

$$\delta\theta_{i,j} = \int_0^{l_{i,j}} \frac{M_{i,j}}{EI_i}dx \quad (3)$$

then

$$x_{i,j+1} = x_{i-1,j+1} + \delta x_{i,j} + l_{i,j}cos(\theta_{i,0} + \sum_{k=1}^{i-1}\delta\theta_{k,j}) \quad (4)$$

$$y_{i,j+1} = y_{i-1,j+1} + \delta y_{i,j} + l_{i,j}cos(\theta_{i,0} + \sum_{k=1}^{i-1}\delta\theta_{k,j}) \quad (5)$$

where $N_{i,j}$ and $V_{i,j}$ are the normal and transverse forces respectively and $M_{i,j}$ is the reaction moment acting on the i^{th} member. $Fx_{i,j}$ and $Fy_{i,j}$ are pseudo forces in the directions of global frame (OX, OY). Elastic modulus, *E*, and the shear modulus, *G*, are kept fixed through the deformation. The length of i^{th} member is denoted as $l_{i,j}$ while A_i stands for the its area and I_i represents the moment of area of that member. Note that $\delta\theta_{i,j}$ accounts for the change in the normal direction of the tip with respect to the local frame (Ox,Oy).

Each compliant member brings three deformation equations (equations 1 - 3). In addition, static equilibrium equations are employed to calculate the internal reaction forces *N*, *V* and moment *M*. These equations are combined with the equations of the constraints in the deformation (shown in Fig.2) and solved simultaneously. For a mechanism of n compliant members, r total members and c constraints the following augmented matrix equation is formed:

$$u^T = [\delta x_{1,j}, \cdots, \delta x_{n,j}, \delta y_{1,j}, \cdots, \delta y_{n,j}, \delta\theta_1, \cdots, \delta\theta_n, M_1, \cdots, M_r, N_1, \cdots, N_r, V_1, \cdots, V_r]^T \quad (6)$$

$$K = \begin{bmatrix} k_{11} & \cdots & k_{1m} \\ \vdots & \ddots & \vdots \\ k_{m1} & \cdots & k_{mm} \end{bmatrix}$$

$$K \times u = 0 \quad (7)$$

where *m* is the total number of equations involved which is equal to the size of the vector of variables, u, shown above. The matrix components, $k_{i,j}$, are determined by those *m* equations. A proper model should yield a square matrix of full rank guaranteeing a unique solution.

For an accurate estimation on the deformation, the model of the structure is solved by a numeric algorithm capable of performing nonlinear analysis. Castigliano's theorem has been applied in compliant structure synthesis [25], [24] in order to derive a direct mathematical expression for the target performance qualifier. Unlike those works, the final state of the compliant body is calculated through iterations updating the status of the body and increasing the load after each iteration. The flowchart in Fig. 3 summarizes the algorithm of that iterative method. When the deformations on the body are significantly high, such an iterative method mitigates the errors caused by altering moment arms and normal directions of members. As the target output displacement, d_{out}, is attained, the iteration stops and the qualifiers: amplification factor, *A*, output stiffness, k_{out}, and total strain energy, *SE*, are derived for performance evaluation as shown in the flowchart. Note that the output stiffness, k_{out}, is the inverse of sensitivity. The amount of force added at each iteration is set by the variable: *increment* as shown in Fig. 3.

The established model employs a similar method as finite element analysis softwares, yet there are two advantages in choosing such a customized routine. The algorithm described here is faster than finite element analysis packages because it deals with an assembly of fewer numbers of elements, only the beams, instead of an n-node mesh. Computing the final state of a typical configuration of the basis mechanism takes around 0.5 sec on a platform of Intel i7 @2.80GHz processor, 6.00 GB RAM and 64-bit operating system with MATLAB (R2010a) software. Also, FEA programs are not suitable for analyses made by varying several parameters.

A major limitation for this method is that it assumes a fixed elastic modulus throughout the whole deformation, although the stress-strain relationship is not linear for plastics even in

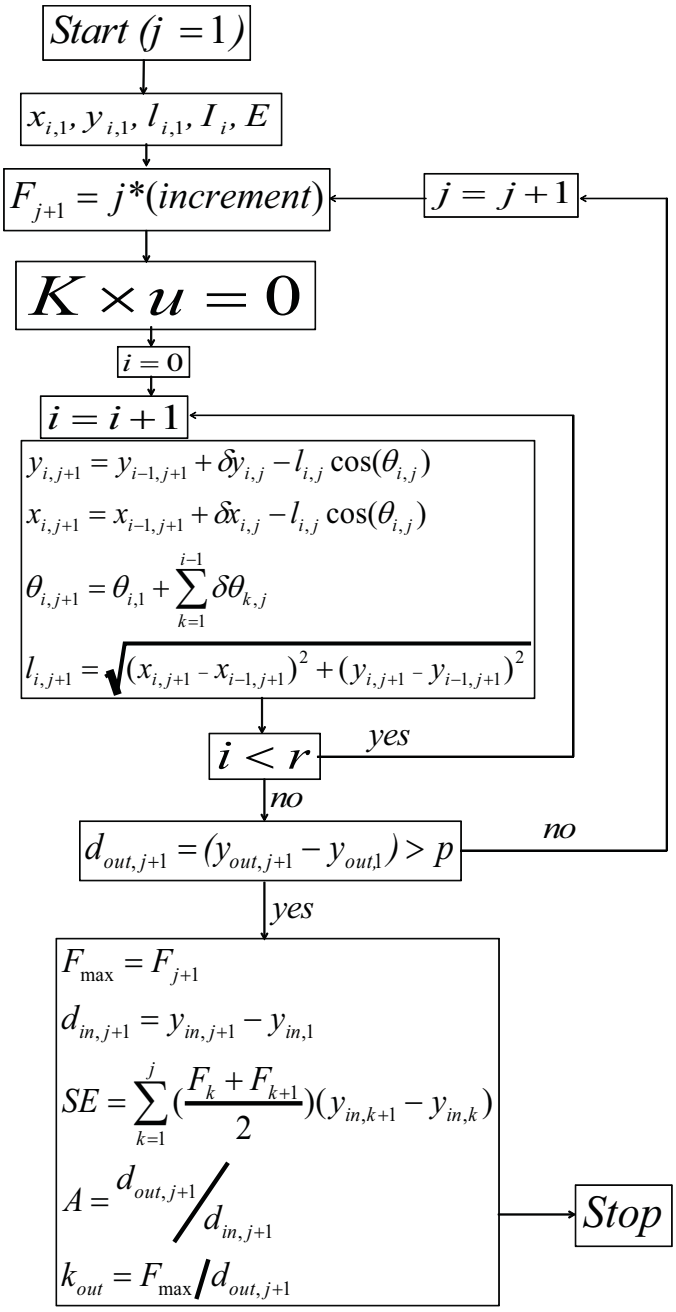

Fig. 3. Flowchart of the iterative method developed for the nonlinear analysis of a compliant mechanism. The variables updated at each iteration are expressed with two subscripts: *i* for the member and *j* for the iteration number. *u* is the vector of variables while *K* is the corresponding square matrix as described in (7). The target output displacement is denoted by *p* and the total number of members is *r*. The subscripts *out* and *in* refers to the output port and input port of the structure respectively.

the elastic range. Given the range of the stresses on the structure during the deformation, a representative fixed modulus was assumed. (See Appendix B for a detailed discussion on the selection of elastic modulus.)

In this work the hysteresis, denoted by *H*, is defined as:

$$H = \frac{max(\Delta f)}{F_{max}} \tag{8}$$

so as to have it resemble the precision of a reading on a

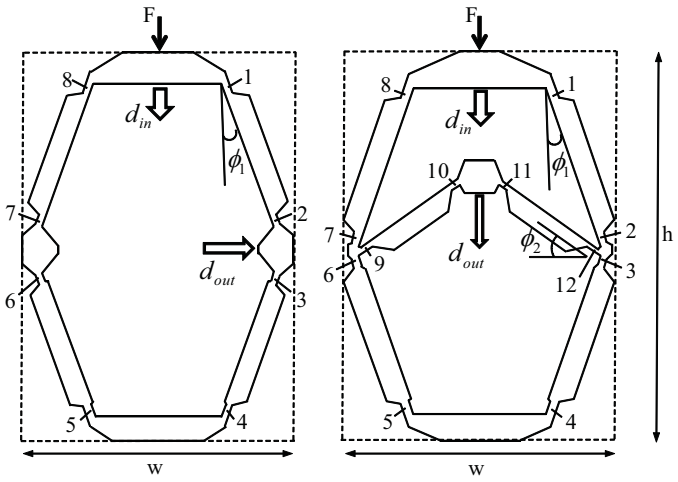

Fig. 4. Full models of the basis mechanism (on the left), the proposed compliant mechanism (on the right). The hinges on the bodies are numbered. The footprint area for the mechanisms are defined by the parameters *h* and *w* as height and width respectively.

sensor. Δf stands for the largest gap between the outputs of the same input in the reverse directions of a loading-unloading experiment and F_{max} is the output range of that experiment.

III. Analysis

A. Numerical Study

The topology of the proposed design is analyzed by varying several geometric parameters in an attempt to evaluate all possible configurations within the same footprint area. The purpose of this type of analysis is to find out how the sensitivity and precision of a sensor are affected by the amplification factor. Possible trade-offs on the performance characterization are observed while optimal configurations for sensitivity and precision are derived. The performance of allowable configurations of the proposed mechanism is compared to a primitive basis mechanism that has a simpler topology.

By definition, the proposed compliant structure should yield 1 mm of output deflection within a footprint area of 25 mm in width and 30 mm in height. A hexagonal structure of the same total area is selected as the basis for comparison. Significant geometric parameters on the proposed and basis mechanisms as well as the frame of the predefined footprint area are shown in Fig.4. Note that the chosen basis mechanism is the proposed mechanism without the middle branch that connects the two vertical sides.

The geometric parameters ϕ_1 and ϕ_2, shown in Fig.4, are selected as independent variables while the dimensions of the hinges are kept fixed. Based on the selected ϕ_1-ϕ_2 couple and hinge dimensions the link lengths are generated. The width of each link is adjusted so as to secure its rigidity and eliminate unwanted deformations. For a given ϕ_1, each (ϕ_1,ϕ_2) configuration of the proposed design is compared to the corresponding basis mechanism with angle ϕ_1. The comparisons are based on the resultant performance qualifiers: amplification ratio, output stiffness (k_{out}) and strain energy (*SE*). This procedure is repeated for two cases having different

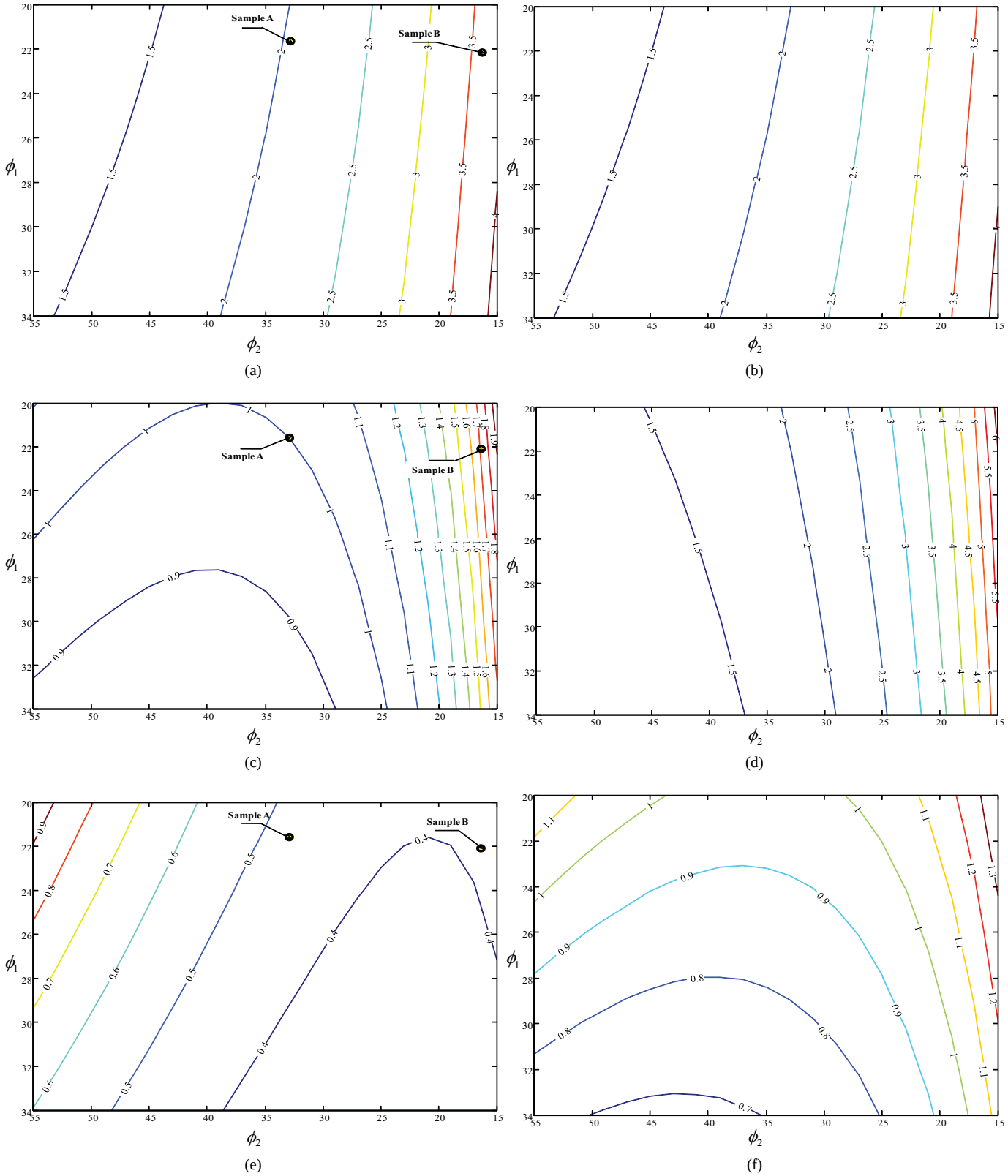

Fig. 5. Contour plots showing the ratio of performance qualifiers of the proposed and basis mechanisms. Two configurations that were tested are shown by dots on the corresponding plots. a) The ratio of amplification factor of the proposed mechanism to that of corresponding basis design for the 05-03 case. A value more than 1 means that the amplification ratio of the proposed design is higher. b) The ratio of amplification factor values for the 03-03 case. c) The ratio of output stiffness of the proposed mechanism to that of corresponding basis design for the 05-03 case. A value less than 1 means that the proposed design has a higher sensitivity at that configuration. d) The ratio of output stiffness values for the 03-03 case. e) The ratio of strain energy of the proposed mechanism to that of corresponding basis design for the 05-03 case. A value less than 1 means that strain energy of the proposed design is smaller at that configuration. f) The ratio of strain energy values for the 03-03 case.

sets of hinges. In the first case (05-03 case), the hinges on the side bars (hinges 1-8 in Fig.4, 0.5 mm wide) are thicker than those in the middle branch (hinges 9-12 in Fig.4, 0.3 mm wide); whereas in the second case (03-03 case) all hinges are identical (0.3 mm wide). The former case represents a structure with a more flexible middle branch compared to the side bars; while in the latter; all hinges are made as flexible as possible considering the manufacturing constraints.

The contour plots in Fig. 5 demonstrate the ratios of the qualifiers of the proposed mechanism over those of the basis mechanism. A value greater than 1 means the proposed design exceeds the basis mechanism in that performance qualifier. The figures 5a, 5c and 5.e belong to 05-03 case amplification, output stiffness and strain energy respectively. Sensitivity of the sensor is reduced with a higher amplification factor as seen in the parallel relation between the amplification factor, Fig. 5a, and output stiffness, Fig. 5c. On the other hand, the total strain energy absorbed by the structure, Fig. 5e, decreases as the amplification factor is increased. As shown by the contours in Fig. 5, the proposed design is generally more advantageous than the basis mechanism in the strain energy aspect, yet, only a certain number of ϕ_1-ϕ_2 couples yield a lower output stiffness, hence a better sensitivity. Dots on the plots represent the sample configurations tested.

The relation between amplification factor and strain energy changes when a different set of hinges is implemented. As the dimensions of the hinges are kept identical (03-03 case) the pattern in the contour plots alternated as shown in Fig. 5b, 5d and 5f. In this case, the strain energy is not monotonically decreasing with an increasing amplification factor. The sensitivity of the sensor still drops as the amplification increases. The basis mechanism is better with regard to sensitivity for most configurations while a certain number of ϕ_1-ϕ_2 selections of the proposed mechanism attain a lower strain energy, hence a better precision than the basis mechanism.

B. Experimental Validation

The accuracy of the described iterative method and the validity of the arguments made via the analysis are tested by loading-unloading experiments performed on three specimens: a particular configuration of the basis mechanism and two corresponding configurations of the proposed mechanism with different amplification factors. Deformations of the samples, estimated by the analytical method, were compared to the experimental results.

The configuration selection of the samples was made using the data obtained by the analysis presented here. The basis mechanism sample was selected to have an amplification factor of 1 (i.e. no amplification). One of the samples of the proposed mechanism, sample A, has a similar output stiffness as the basis mechanism; whereas the other, sample B, achieves a higher amplification factor with a higher output stiffness yet much lower strain energy compared to the basis mechanism. The dimensions of the hinges on the tested mechanisms were selected to be the 05-03 case since the difference between the proposed and basis mechanisms is more significant in that case. Table I presents the independent parameters which define

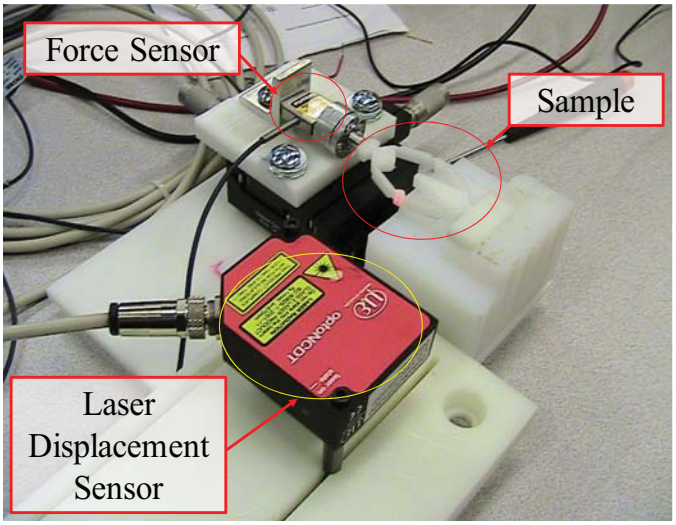

Fig. 6. Experimental setup showing the displacement and force measuring apparatus

the amplification factor of the manufactured samples. All samples are cut from a 5.1 mm thick delrin sheet using a water jet cutter. Due to the inaccuracies in the manufacturing process the values of those parameters and dimensions of the hinges were not perfectly identical to those intended. A detailed list of the measured thickness values of the hinges of the tested samples is given in Appendix B. The analytical model is updated considering the measured hinge dimensions. In the experiments, a known displacement was applied on the input port of the samples using Newport 460A X-stages. The applied force at the input port was measured by a Futek LSB200 JR S-Series load cell and the deflection at the output port was measured using optoNCDT 1300 laser displacement sensor. Fig. 4 shows the input and output ports of each sample and a picture of the experimental setup for the basis mechanism is shown in Fig.6. In the first experiment, performed on the basis mechanism, an effective elastic modulus constant was determined to be 2.3 GPa. The same empirical value was applied to all other cases. A more detailed explanation on the elastic modulus determination is given in Appendix B.

Since plastic, rubber-like materials exhibit altering deformation curves after each time being loaded, several loading-unloading cycles have been performed on the samples so as to have a fair discussion on their mechanical performances. The tests indicated no sign of softening or major repeatability errors. Details on the loading-unloading cycles of the experimental procedure and a discussion on the altering deformation behaviors of plastics due to stress relaxation, and Mullins effect is given in Appendix C. Fig.7 presents the results of the analytical method and the experimental data. The resultant sensitivity, strain energy and hysteresis of each specimen, calculated using the experimental data as well as the estimations of the analytical model, are given in Table II. The values calculated by the analytical method are given in parentheses. Analytical model data follows the same deformation trends as the experimental data, yet the analytical model appears stiffer than the samples. One of the main reasons for the error is

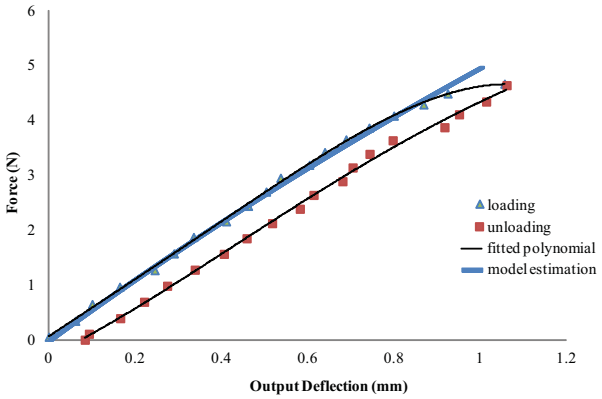

(a)

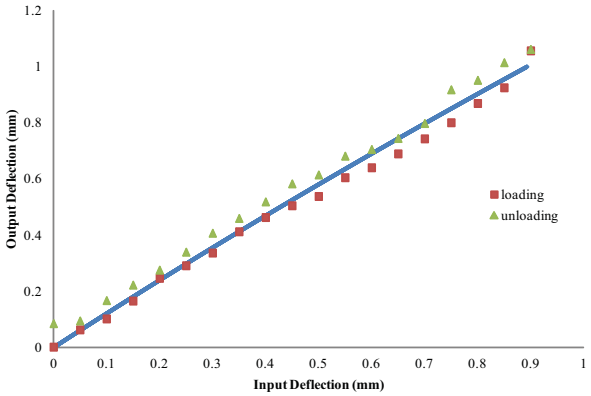

(b)

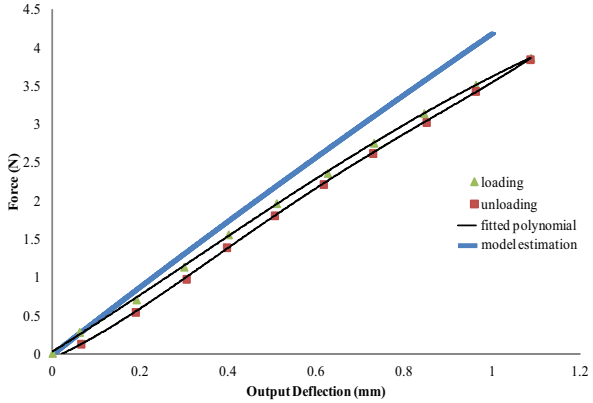

(c)

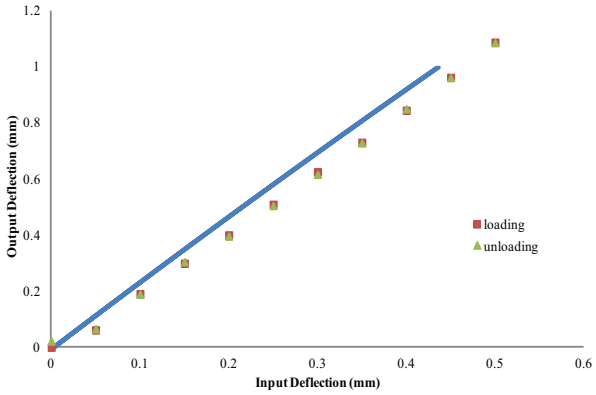

(d)

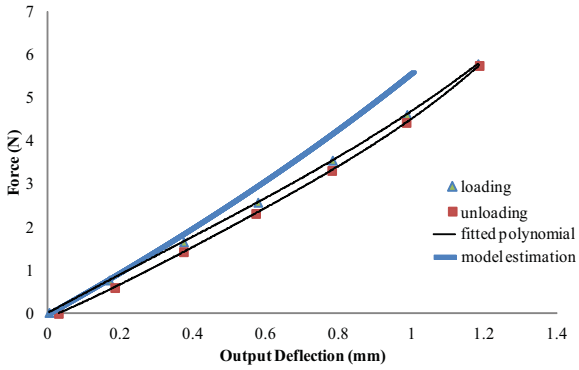

(e)

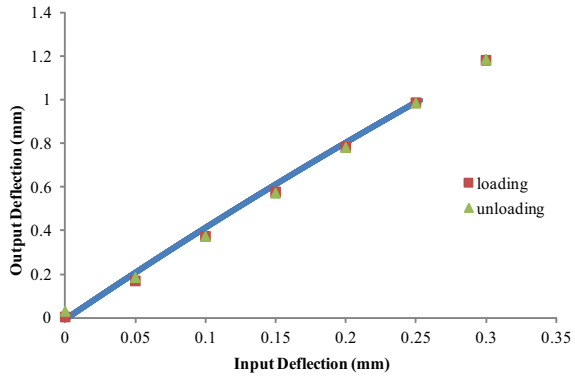

(f)

Fig. 7. Experimental results (dotted) in comparison with the calculations of the analytical method. On the force vs. deformation plots, 4^{th} order polynommials are fitted to the experimental data points. a,b) Deformation of the basis mechanism c,d) Deformation of sample A, the one with a moderate amplification factor e,f)Deformation of sample B, the one with a high amplification factor

TABLE I
SIGNIFICANT PARAMETERS OF THE SELECTED CONFIGURATIONS

Model	θ_1	θ_2
Basis Mechanism	22°	-
Sample *A* (Modarate Amplification Mechanism)	21°	34°
Sample *B* (High Amplification Mechanism)	22°	17.2°

TABLE II
PERFORMANCE QUALIFIERS OF THE TESTED CONFIGURATIONS

Model	Strain Energy in mJ	Hysteresis	Sensitivity in mm/N	Overall Quality (SNR)
Basis Mechanism	2.187 (2.385)	0.135	0.227 (0.202)	1.682
Sample A- Modarate Amplification Mechanism	0.815 (0.941)	0.046	0.281 (0.239)	6.109
Sample B- High Amplification Mechanism	0.550 (0.684)	0.036	0.204 (0.178)	5.667

the inaccuracy in the manufacturing process. 2D power cutting tools like water jet cutter often results in a V-shaped cut profile which makes it impossible to determine the true geometry of a hinge and the stiffness of a compliant mechanism is very sensitive to the thickness of the hinges. The samples involve more than 10 hinges per structure and due to the random nature of the manufacturing errors the symmetry on the structures is not guaranteed. The error could also be ascribed to the rigid boundary conditions which are not perfectly realistic and the problem of non-linear stress-strain curve of the material i.e. variable elastic modulus. The method still estimates the deformation of a mechanism with several hinges with an error about 20%, which is not severely high compared to similar experimental works [26].

The experiments confirmed the parallel relation between hysteresis and strain energy predicted by our analysis as shown in Table II. Sample B has the least hysteresis, yet it is poorer with regard to sensitivity than the basis mechanism. A slightly higher amount of hysteresis could be traded for a better sensitivity by selecting sample A. It is superior to the basis mechanism in both sensitivity and precision. If the ratio of sensitivity over hysteresis is accepted as a quality indicator for the overall sensing performance, describing the signal-to-noise ratio (SNR) of the sensor, sample A becomes the best among the samples tested. All these experimental results confirm the arguments made using the theoretical analysis.

IV. DISCUSSION

We analyzed our proposed design to improve its sensing performance and characterized its performance with regard to both sensitivity and precision aspects. Rather than exercising a size and shape optimization routine, we compared the advantages of the proposed displacement amplifying compliant mechanism over these of a simpler, low or no-amplifying body. Such a comparison and a variation analysis yielded important insight on the use of displacement amplification on sensors. Depending on the set of hinges, high sensitivity and low hysteresis may become pareto qualifiers leaving a trade-off on the selection of optimal configuration. Displacement amplification can improve the signal-to-noise ratio (SNR) of a sensor by reducing the hysteresis error rather than increasing the sensitivity.

As shown in the analysis of selected cases, the amplification factor raises the stiffness of the structure, making it harder to deform. This is consistent with the fact that amplification mechanisms do not necessarily improve the sensitivity. In the two cases analyzed herein, the proposed design was not significantly better with regard to sensitivity compared to the basis structure. However, its benefits become apparent when the total strain energy is considered. The proposed design reduces the necessary strain energy for an identical output deflection alleviating the hysteresis problem. The range of such advantageous configurations changes with hinge set, since the variations of the sensitivity and strain energy depend on the relative dimensions of the hinges. For the 05-03 case, a limited range of (ϕ_1,ϕ_2) selection yields both an improved sensitivity and precision; whereas for the 03-03 case, (when all the hinges are 0.3 mm), the proposed design cannot improve the sensitivity compared to the basis mechanism. It can, however, enhance the precision for a certain number of configurations.

To the best of our knowledge, there is no perfectly objective, indisputable method for comparing two displacement amplifying compliant mechanisms (DACM) with different topologies taking all performance qualifiers into account. In this work, the analysis of the proposed design is driven by the question: "What is the advantage of our specially designed mechanism over an ordinary, simple body" i.e., is it worth using such a complex structure instead of a simple geometry for force sensing? A hexagonal body was taken to be the basis mechanism for comparison since it allows for a translational displacement at the output port and could be adjusted to low or no amplification configurations. This analysis showed that it is the *hysteresis error* of the force sensor on which a DACM has the biggest impact. Optimizing a topology for sensitivity does not assure a better sensor; since even when it degrades sensitivity, a DACM can still prove to have a better SNR than a basic structure.

The experiments confirmed the outcomes of the analysis showing the trade-off between sensitivity and hysteresis. Among the selected configurations of the proposed design, sample A is superior in both sensitivity and hysteresis to the selected basis structure. On the other hand, sample B is not better in sensitivity compared to the basis mechanism, yet it has a considerably higher SNR mainly because of its mitigated hysteresis error. Our hypothesis on the relation between strain energy and hysteresis was confirmed by the experiments. The numeric estimations made using the analysis are in parallel with the experimental results.

The inaccuracies in the manufacturing process of polymers may yield a structure different from what has been attempted to obtain. This could result in a drastic decrease in the expected performance of an optimal design if its optimality is so sensitive to the geometry of its members. The manufacturing tolerances and robustness of the optimization process should be considered when designing a DACM.

The analysis presented here is insufficient for proposing a genuine objective function that takes the hysteresis of a sensor

into account. The direct numerical relation between strain energy and hysteresis, i.e. the weight of strain energy's effect on hysteresis, is not clear. Hysteresis should be explicitly defined by the design parameters for a helpful objective function which brings SNR into consideration. Also, the calculation method utilized in this study assumes a constant elastic modulus, whereas, in reality that of a plastic material such as delrin is not perfectly constant. An advanced method that could take varying elastic modulus without compromising other abilities of the existing algorithm could achieve an improved accuracy.

V. Conclusion

An MRI compatible force sensor, that is comprised of a displacement amplifying compliant mechanism, introduced in an earlier work [33], was analyzed for its sensitivity and precision. The results of the analysis were utilized to enhance the SNR of the proposed sensor. An iterative method capable of performing nonlinear analysis, faster than commercial softwares and applicable to any iterative study was established. The effects of displacement amplification on the sensitivity and precision of the proposed force sensor were investigated and the proposed design was compared to a simple, low, or non-amplification mechanism. The analysis on the topology of the proposed compliant mechanism showed that an aggressive amplification raises the stiffness of the structure, degrading the sensitivity; yet it also lowers the strain energy absorbed by the structure, mitigating the hysteresis problem. The optimal configurations for sensitivity and precision vary with the stiffness values of the set of hinges on the mechanism. Predictions on the optimal configurations made by the analysis were confirmed by the experiments conducted on three samples of different configurations. An error of about 20% was observed compared to the analytical method which can be ascribed to the inaccuracies in the manufacturing technique, water-jet cutting.

Rather than optimizing the topology for a certain objective function as practiced in previous works, the analysis done herein provides an insight on the benefits of displacement amplification. The use of a DACM as a sensor should not be viewed only with regard to the aspect of sensitivity. DACM topologies with a lower sensitivity may still improve the performance of sensors since the amplification of displacement can reduce the problem of hysteresis, enhancing the signal-to-noise ratio of a sensor. Lower hysteresis error, hence better precision, is the key factor that makes a displacement amplifying topology advantageous against a simple, flexible, low-stiffness body. Experiments on selected configurations of our proposed design showed that SNR of the proposed force sensor could be up to 3-4 times that of a non-amplifying structure.

Appendix

A. Principle of the Optic Sensing

The sensing principle of the proposed MRI compatible force sensor is based on translation of a mirror that faces to a fiber optic cable as shown in Fig. 1. A single fiber optic cable both emits light towards the mirror and collects the light rays reflected from the mirror. As the gap between the fiber optic cable tip and the mirror changes, the amount of light energy collected by the cable varies. The collected light energy is converted to voltage by a fiber optic circuitry [34].

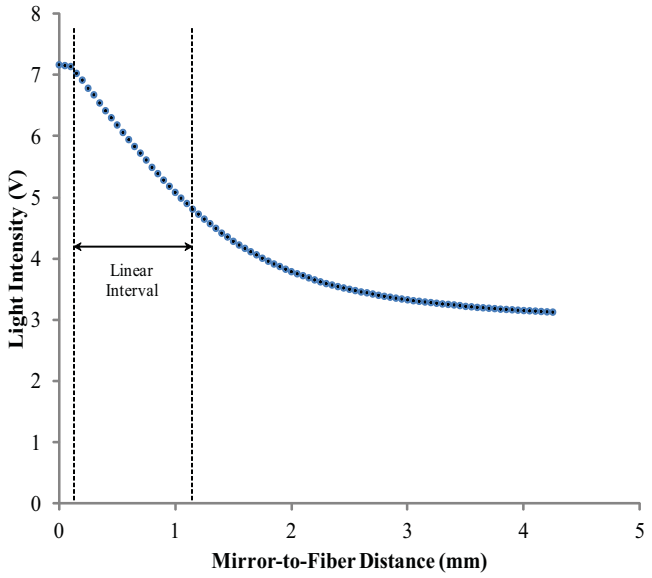

Fig. 8. Light intensity vs. the distance between the mirror and the fiber tip. The intensity of light rays was measured in voltage through a photovoltaic circuitry. The output changes in a linear fashion for a 1 mm of displacement interval.

The relation between the mirror-to-fiber distance and the output voltage of the optic circuitry has been realized by an experiment. A magenta mirror made of silicon is mounted on a single axis translation stage and aligned to a plastic fiber optic cable of 0.9 mm diameter. The light source is chosen to be a red laser of 850 nm wavelength. While the mirror was translated towards the fiber optic cable, intensity of the reflected light was measured using a photovoltaic circuitry. As Fig. 8 presents, within a certain interval marked by the dashed lines (0.2-1.2 mm) the relation between the output voltage and mirror-to-fiber distance appears to be linear. That 1 mm wide interval determined the range of operation of the proposed compliant design in order to preserve the linearity between the input force and output voltage.

B. Details on Manufactured Samples

The thickness values of the hinges on the manufactured samples are given in Table III. These values are estimations based on rough measurements on the thickness of the members. Since the V-shaped cut profiles on the hinges are not exactly known, these values are prone to result in errors. The hinges are represented by the numbers assigned in Fig. 4.

Another issue for the accuracy of the method described here is the assumed elastic modulus. 2.3 GPa was assumed using the first loading test performed on the basis mechanism and that value was applied to the model of the proposed design as well. To verify that assumption a tensile strength test on the material of the samples, delrin, is performed. Fig. 9 shows the entire stress-strain curve of the tensile strength test and the

TABLE III
THICKNESS VALUES OF THE HINGES ON THE SAMPLES

Hinge Number	Basis Mechanism (mm)	Sample A (Modarate Amplification Mechanism) (mm)	Sample B (High Amplification Mechanism) (mm)
1 0.58	0.50	0.52	
2	0.54	0.48	0.55
3	0.54	0.48	0.55
4	0.54	0.52	0.53
5	0.53	0.52	0.52
6	0.53	0.51	0.51
7	0.50	0.51	0.51
8	0.58	0.50	0.50
9	-	0.25	0.26
10	-	0.30	0.30
11	-	0.30	0.31
12	-	0.25	0.26

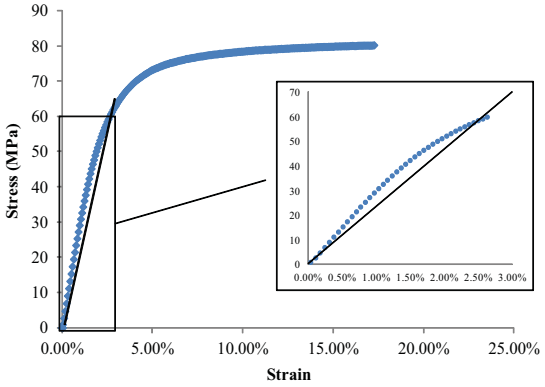

Fig. 9. Stress vs. strain data of delrin with with 2.3 GPa constant elastic modulus line. The elastic region of the stress vs. strain data is zoomed.

portion of that curve which matches to the 2.3 GPa constant elastic modulus line.

The stress distribution over the beam members of the basis and proposed mechanisms has been realized utilizing the relevant methods given in Hibbeler's book and disregarding the stress concentration [35]. The stress concentration on the samples depends on the cut profile of the hinges as well as the surface quality of the cut; therefore there is not enough information for an accurate estimate on the concentration effects. A maximum stress of 40 MPa was calculated on the tested samples which is on the order of what is needed for a valid elastic modulus estimation of 2.3 GPa, considering a moderate concentration factor for the hinges which are classified as flat beams with opposing notches [36].

C. Loading Cycles on Plastic Samples

In order to decouple the hysteresis error from other elements such as Mullins effect, softening and stress relaxation, a certain procedure was followed for all specimens. Firstly, three consecutive loading-unloading cycles were performed on the specimens. A maximum output displacement of 1 mm was aimed in each cycle, and was completed in less than two minutes, depending on the amplification factor of the mechanism being tested. Following the consequtive loadings, the specimens were allowed to rest for 15 minutes for recovery.

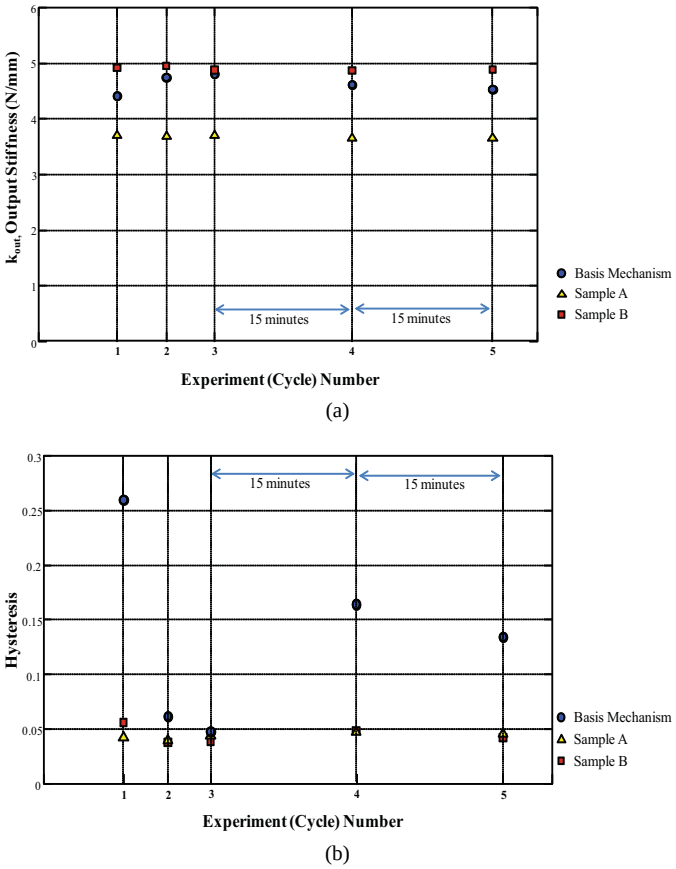

Fig. 10. Performance of specimens after 5 loading-unloading cycles a) Output stiffness of the samples b) Hysteresis levels for each cycle

After the recovery, a fourth run was completed. The fourth run was followed by another recovery session of 15 minutes and a fifth run. Fig. 10 shows the force-deformation data for the basis mechanism.

As shown in Fig. 10b, the hysteresis error is mitigated after the repetitive cycles but partially recovered after a certain recovery session. However, there is no indication for softening or a drop in stiffness caused by these cycles, as shown in Fig. 10b. The hysteresis error after recovery is repeatable for the specimens and the stiffness of the samples did not change significantly after multiple full-scale loadings. For the discussion in this article, the fifth runs were taken into account so as to get rid of the effects of consecutive loadings. Since the specimens presented no softening during the process, the Mullins effect was ruled out [37], [38].

REFERENCES

[1] F. A. Jolesz, P. R. Morrison, S. J. Koran, R. J. Kelley, S. G. Hushek, R. W. Newman, M. P. Fried, A. Melzer, R. M. M. Seibel, and H. Jalahej, "Compatible instrumentation for intraoperative mri: Expanding resource," *Journal of Medical Imaging*, vol. 8, pp. 8–11, February 1998.

[2] G. S. Fischer, I. Iordachita, C. Csoma, J. Tokuda, S. P. DiMaio, C. M. Tempany, N. Hata, and G. Fichtinger, "Mri-compatible pneumatic robot for transperineal prostate needle placement," *IEEE/ASME Transactions on Mechatronics*, vol. 13, no. 3, pp. 295–305, 2008.

[3] S. Song, N. B. Cho, G. Fischer, N. Hata, C. Tempany, G. Fichtinger, and I. Iordachita, "Development of a pneumatic robot for mri-guided transperineal prostate biopsy and brachytherapy: New approaches," in *Proc. IEEE Int Robotics and Automation (ICRA) Conf*, pp. 2580–2585, 2010.

[4] R. Gassert, R. Moser, E. Burdet, and H. Bleuler, "Mri/fmri-compatible robotic system with force feedback for interaction with human motion," *IEEE/ASME Transactions on Mechatronics*, vol. 11, no. 2, pp. 216–224, 2006.

[5] A. Khanicheh, A. Muto, C. Triantafyllou, B. Weinberg, L. Astrakas, A. Tzika, and C. Mavroidis, "Mr compatible erf driven hand rehabilitation device," in *Proc. 9th Int. Conf. Rehabilitation Robotics ICORR 2005*, pp. 7–12, 2005.

[6] Z. Tsz Ho Tse, H. Elhawary, A. Zivanovic, M. Rea, M. Paley, G. Bydder, B. L. Davies, I. Young, and M. U. Lamperth, "A 3-dof mr-compatible device for magic angle related in vivo experiments," *IEEE/ASME Transactions on Mechatronics*, vol. 13, no. 3, pp. 316–324, 2008.

[7] R. Gassert, D. Chapuis, H. Bleuler, and E. Burdet, "Sensors for applications in magnetic resonance environments," *IEEE/ASME Transactions on Mechatronics*, vol. 13, no. 3, pp. 335–344, 2008.

[8] P. Puangmali, P. Dasgupta, L. D. Seneviratne, and K. Althoefer, "Miniaturized triaxial optical fiber force sensor for mri-guided minimally invasive surgery," in *Proc. IEEE Int Robotics and Automation (ICRA) Conf*, pp. 2592–2597, 2010.

[9] D. Chapuis, R. Gassert, L. Sache, E. Burdet, and H. Bleuler, "Design of a simple mri/fmri compatible force/torque sensor," in *Proc. IEEE/RSJ Int. Conf. Intelligent Robots and Systems (IROS 2004)*, vol. 3, pp. 2593–2599, 2004.

[10] M. Tada, S. Sasaki, and T. Ogasawara, "Development of an optical 2-axis force sensor usable in mri environments," in *Proc. IEEE Sensors*, pp. 984–989, 2002.

[11] M. Tada and T. Kanade, "Design of an mr-compatible three-axis force sensor," in *Proc. IEEE/RSJ Int. Conf. Intelligent Robots and Systems (IROS 2005)*, pp. 3505–3510, 2005.

[12] N. Takahashi, M. Tada, J. Ueda, Y. Matsumoto, and T. Ogasawara, "An optical 6-axis force sensor for brain function analysis using fmri," in *Proc. IEEE Sensors*, vol. 1, pp. 253–258, 2003.

[13] U. Tan, B. Yang, R. Gullapalli, and J. P. Desai, "Triaxial mri-compatible fiber-optic force sensor," *IEEE Transactions on Robotics*, vol. 27, no. 1, pp. 65–74, 2011.

[14] J. F. Schenck, "The role of magnetic susceptibility in magnetic resonance imaging: Mri magnetic compatibility of the first and second kinds," *Medical Physics -Lancaster PA-*, vol. 23, no. 6, pp. 815–850, 1996.

[15] L. L. Howell, *Compliant Mechanisms*. Wiley-Interscience, 2001.

[16] C. B. W. Pedersen, T. Buhl, and O. Sigmund, "Topology synthesis of large-displacement compliant mechanisms," *International Journal for Numerical Methods in Engineering*, vol. 50, no. 12, pp. 2683–2705, 2001.

[17] C. B. W. Pedersen and A. A. Seshia, "On the optimization of compliant force amplifier mechanisms for surface micromachined resonant accelerometers," *Journal of Micromechanics and Microengineering*, vol. 14, no. 10, pp. 1281–1293, 2004.

[18] S. R. Deepak, M. Dinesh, D. K. Sahu, and G. K. Ananthasuresh, "A comparative study of the formulations and benchmark problems for the topology optimization of compliant mechanisms," *Journal of Mechanisms and Robotics*, vol. 1, 2009.

[19] A. Saxena and G. Ananthasuresh, "On an optimal property of compliant topologies," *Structural and Multidisciplinary Optimization*, vol. 19, pp. 36–49, 2000. 10.1007/s001580050084.

[20] O. Sigmund, "On the design of compliant mechanisms using topology optimization*," *Mechanics of Structures and Machines*, vol. 25, no. 4, pp. 493–524, 1997.

[21] L. Yin and G. K. Ananthasuresh, "Design of distributed compliant mechanisms," *Mechanics Based Design of Structures and Machines*, vol. 31, no. 2, pp. 151–179, 2003.

[22] J. H. Kim, S. H. Kim, and K. Y. K., "Development of a piezoelectric actuator using a three-dimensional bridge-type hinge mechanism," *Review of Scientific Instruments*, vol. 74, pp. 2918–2924, May 2003.

[23] M. B. Parkinson, B. D. Jensen, and K. Kurabayashi, "Design of compliant force and displacement amplification micro-mechanisms," in *ASME 2001 Design Engineering Technical Conferences*, 2001.

[24] Y. Guo, L. Wei, W. Yu-Qiao, Y. Xue-Feng, and Y. Ling, "Kinematics analysis of bridge-type micro-displacement mechanism based on flexure hinge," in *Information and Automation (ICIA), 2010 IEEE International Conference on*, pp. 66 –70, june 2010.

[25] N. Lobontiu and E. Garcia, "Analytical model of displacement amplification and stiffness optimization for a class of flexure-based compliant mechanisms," *Computers & Structures*, vol. 81, no. 32, pp. 2797 – 2810, 2003.

[26] N. Lobontiu, S. N. P. Jeffrey, E. Garcia, and M. Goldfarb, "Corner-filleted flexure hinges," *Journal of Mechanical Design*, vol. 123, no. 3, pp. 346–352, 2001.

[27] Q. Xu and Y. Li, "Analytical modeling, optimization and testing of a compound bridge-type compliant displacement amplifier," *Mechanism and Machine Theory*, vol. 46, no. 2, pp. 183 – 200, 2011.

[28] G. Krishnan and G. K. Ananthasuresh, "Evaluation and design of displacement-amplifying compliant mechanisms for sensor applications," *Journal of Mechanical Design*, vol. 130, no. 10, p. 102304, 2008.

[29] Z. Wang and H. Hu, "Analysis and optimization of a compliant mechanism-based digital force/weight sensor," *IEEE Sensors Journal*, vol. 5, no. 6, pp. 1243–1250, 2005.

[30] J. N. Gorce, J. W. Hellgeth, and T. C. Ward, "Mechanical hysteresis of a polyether polyurethane thermoplastic elastomer," *Polymer Engineering & Science*, vol. 33, no. 18, pp. 1170–1176, 1993.

[31] A. Granato and K. Lucke, "Theory of mechanical damping due to dislocations," *Journal of Applied Physics*, vol. 27, pp. 583–593, 1956.

[32] U. Tan, B. Yang, R. Gullapalli, and J. P. Desai, "Design and development of a 3-axis mri-compatible force sensor," in *Proc. IEEE Int Robotics and Automation (ICRA) Conf*, pp. 2586–2591, 2010.

[33] M. Turkseven and J. Ueda, "Design of an mri compatible haptic interface," in *Proc. IEEE/RSJ Int Intelligent Robots and Systems (IROS) Conf*, pp. 2139–2144, 2011.

[34] M. Lazeroms, G. Villavicencio, W. Jongkind, and G. Honderd, "Optical fibre force sensor for minimal-invasive-surgery grasping instruments," in *Proc. 18th Annual Int. Conf. of the IEEE Bridging Disciplines for Biomedicine Engineering in Medicine and Biology Society*, vol. 1, pp. 234–235, 1996.

[35] R. C. Hibbeler, *Mechanics of Materials*. Prentice Hall, 7th edition ed., 2008.

[36] D. F. Pilkey, Walter D.; Pilkey, *Peterson's Stress Concentration Factors*. John Wiley & Sons, third ed., 2008.

[37] F. Bueche, "Molecular basis for the mullins effect," *Journal of Applied Polymer Science*, vol. 4, no. 10, pp. 107–114, 1960.

[38] F. Bueche, "Mullins effect and rubber-filler interaction," *Journal of Applied Polymer Science*, vol. 5, pp. 271–281, 1961.